

EXTENSIONAL VISCOSITY OF THERMOPLASTIC TUFF COMPOSITES IN STRETCH FORMING PROCESSES

Henry Fidlow^{1,2}, Thomas A. Cender¹, Pavel Simacek^{1,2}, Shridhar Yarlagadda¹, Suresh G. Advani^{1,2}

¹ Center for Composite Materials, University of Delaware, Newark, DE 19716

² Department of Mechanical Engineering, University of Delaware, Newark, DE 19716

ABSTRACT

Tailored Universal Feedstock for Forming (TuFF) is a novel composite material form consisting of highly aligned short fiber reinforcement. The high degree of alignment allows for fiber volume fractions up to 60% and mechanical performance equivalent to aerospace grade continuous fiber composites. The discontinuous fiber format has demonstrated the ability to allow stretch forming of composite blanks in the fiber direction. This work studies the material behavior during stretch forming to develop constitutive laws for the fiber direction deformation. It is shown that shearing of neighboring fibers through the melt phase thermoplastic matrix imparts a viscous deformation response. Longitudinal fiber direction viscosity was measured as a function of strain, strain-rate, and temperature under various processing conditions. Digital image correlation (DIC) was used to measure the local surface strain data for uniaxial tension tests and derive the extensional viscosity data. A micromechanics model which accounts for polymer properties and microstructure features was formulated to validate the experimentally derived constitutive law.

Keywords: Composite Forming, Thermoplastic, Discontinuous Carbon Fiber, TuFF

Corresponding author: Thomas A. Cender

DOI: (Will be added by SAMPE)

1. INTRODUCTION

In recent years, there has been an influx of interest in thermoplastic aligned discontinuous fiber composites (ADFCs). This newfound attention has resulted from superior formability and recyclability characteristics as compared to continuous fiber composite counterparts [1]. Viability of this market is largely dependent on the ability to accelerate processing speeds, retain high alignment, and reduce costs. Currently, slower production rates have caused continuous fiber composites to outperform ADFCs in commercial markets [1]. In the mechanical realm, it is important that fiber alignment is maximized in ADFCs if they are to compete with continuous fiber composites since better alignment yields higher fiber volume fractions and improved structural properties. Due to the use of discontinuous fibers, ADFCs have the ability to dominate the thermoplastic composite market since they allow for improved drapability, forming of complex part geometries, and recycled fiber usage as compared to the current state-of-the-art.

To address all of these issues, the Center for Composite Materials at the University of Delaware (UD-CCM) has developed a novel composite material form called Tailored Universal Feedstock for Forming (TuFF) consisting of highly aligned discontinuous fiber plies with a fiber volume

Copyright 2022 by Henry Fidlow. Published by Society for the Advancement of Material and Process Engineering with permission.)

SAMPE Conference Proceedings. Charlotte, NA, May 23-26, 2022. Society for the Advancement of Material and Process Engineering – North America.

fraction of 57% and short 3mm fibers [2-4]. Figure 1 shows TuFF from the microstructural view of a single ply up to the macroscopic view of a formed part. Compared to existing state-of-the-art short fiber composites such as HiPerDif and Disco, the strength and stiffness of TuFF has proven far superior [2]. Beyond this, TuFF properties are also on par with existing IM7/8552 continuous fiber composites [5]. When combining these properties with short fibers which enable impressive fiber direction elongation, among other benefits, TuFF presents the potential for innovation in a variety of aerospace applications from thermoforming processes to automated fiber placement and tape laying [6-7].

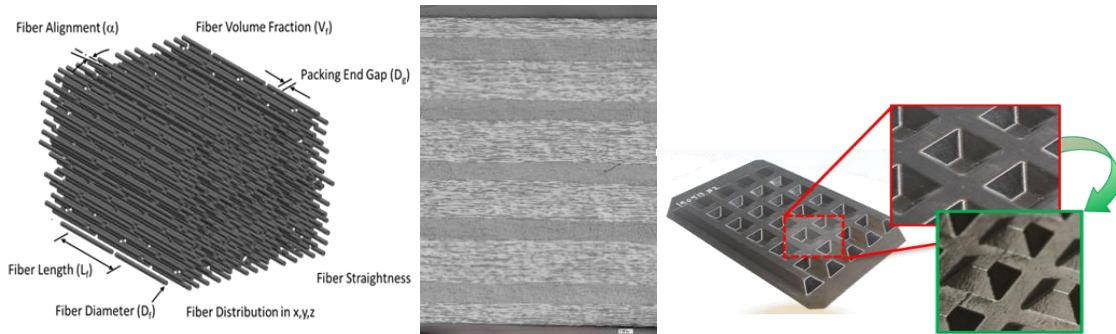


Figure 1. (Left) TuFF fiber scale microstructure [3]. (Center) Cross-section of TuFF laminate structure. (Right) Stretch formed TuFF part [7].

Quasi-isotropic ply sequences, traditionally $[0/45/90/-45]_{ns}$, have previously been used by the UD-CCM to experimentally illustrate TuFF composite formability [7]. However, many aspects of this forming remain unexplored. To better understand the material response to stretch forming, this paper investigates the extensional viscosity of CF-PEI TuFF in the fiber direction to describe the material behavior under applied loads with constitutive laws. Using digital image correlation (DIC) methods to analyze surface strain patterns, non-uniform sample deformation was observed. This information provided more accurate strain data when compared to open loop strain control from the universal testing machine (UTM). Operating at strain rates and temperatures indicative of real forming conditions, extensional viscosity was fit to a power law fluid model to describe the material response. In addition, a rheological study of polymer shear viscosity was conducted using frequency oscillations. This data was fit to a Carreau model which describes the shear thinning behavior of thermoplastic polymers at high shear rates but accounts for a Newtonian plateau at low shear rates. Finally, an existing micromechanics model was used to relate extensional viscosity of an ADFC with polymer shear viscosity under Newtonian assumptions. Using experimentally measured polymer shear viscosity along with the extensional viscosity described above, this model was used to validate the experimental results and the constitutive model obtained.

There are two main catalysts for this work. The first is to develop a physical understanding of the microstructural evolution of TuFF during stretch forming. Simacek and Advani developed a simulation to leverage random fiber lengths, overlaps, and end gaps to predict relative viscosity for similar ADFCs [8]. Although robust in its considerations, important factors such as thermally introduced porosity were not included. Since this could significantly affect model accuracy, experimentation is necessary to verify simulation results. By investigating TuFF extensional viscosity using DIC methods, non-uniform behavior can be further characterized and a continuum approach can be compared to previous works. At the same time, it is extremely valuable to develop an FE material forming simulation for the TuFF material. Obtaining the constitutive laws of TuFF

in the fiber direction is a crucial step in developing such a simulation, since the fiber direction is the predominant factor in describing deformational response. This work is an important step toward developing a complete predictive simulation for TuFF in stamp forming processes.

2. EXPERIMENTATION

The strength characteristics of a unidirectional fiber reinforced composite are highly anisotropic. It is of chief concern to look at the fiber direction when assessing these composites since it is the dominant contributing factor in describing the stamp forming of quasi-isotropic laminates. Given the interest in TuFF specifically, extensional viscosity (η_L) was calculated under strain rate controlled tension using a UTM. Experiments were performed on a single ply of CF-PEI TuFF, with extension acting in the fiber direction. The plies had a fiber areal weight of 120 gsm and a thickness of 0.125 mm/ply. Together, these parameters produced a fiber volume fraction of 57%.

2.1 TuFF Sample Preparation

TuFF test samples were comprised of IM7 carbon fibers impregnated with ULTEM1000 PEI. The fibers were 5 μm in diameter and cut to 3 mm in length to yield a fiber aspect ratio of 600. This low aspect ratio was instrumental to improving formability of the material. PEI was selected as the matrix because of its aerospace grade properties, high temperature resistance, and amorphous structure which simplifies testing at elevated temperatures. The consolidation process was conducted on the 16" x 16" ply at 300 psi and 330°C in a hot press.

After consolidation, samples were cut into 7" x 1" slips using a slot grinder. With the addition of end tabs, this yielded a 3" gap between grips. Once cut to final dimensions, the width and thickness were measured at the centerline of the samples. When combined with transverse strain data, incompressibility assumptions, and force measurements from the load cell, stress was calculated.

Typically, transverse strain is calculated as a function of longitudinal strain (ϵ_L) based on the strain control of the UTM and incompressible assumptions of the material. This is shown in Equation 2.

$$\epsilon_L + \epsilon_{22} + \epsilon_{33} = 0 \quad (1)$$

$$\epsilon_{22} = \epsilon_{33} = -\frac{1}{2}\epsilon_L \quad (2)$$

If initial specimen dimensions are known, width and thickness can be calculated as long as ϵ_L is also provided. However, in ADFCs, there is much greater variability in properties as compared to isotropic materials due to fiber misalignment and randomness introduced through fiber end gaps/overlaps [8]. Given these additional issues, it is important to alter the method of strain measurement to improve the accuracy of collected data.

2.2 Digital Image Correlation

To address the issue of non-uniformity, digital image correlation (DIC) analysis was implemented. DIC analysis required further preparation of these samples through surface speckling of the ungripped section. Since the TuFF material itself was black, a single layer of high temperature white spray paint was applied to the middle 3" of one side of the sample in a speckle pattern, as shown in Figure 2. Target surface area coverage was around 50% of the middle section, with speckle sizes on the order of 0.1-1 mm.

DOI: (Will be added by SAMPE)



Figure 2. Prepared TuFF samples after cutting and speckling, with a speckled length and width of 3" and 1" respectively. After a drying cycle, the samples are ready to be tested.

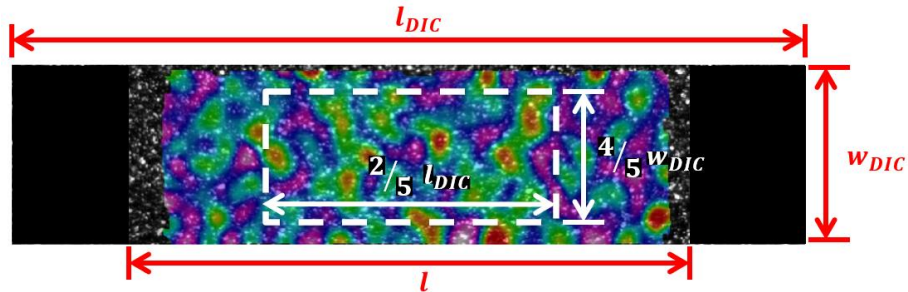


Figure 3. DIC analysis of longitudinal strain field for one frame in VIC-2D. The dashed white border depicts the data that was used in calculating average strain rate for the frame. The image size has dimensions of $l_{DIC} = 4.114''$ and $w_{DIC} = 0.639''$.

DIC analysis was conducted in VIC-2D. Applying Hencky strain conditions with an image size of 41 pixels and a step size of two pixels, local strain was measured across the surface for each image and later reduced to the gauge section depicted in Figure 3.

2.3 Uniaxial Tension

The final step before the samples were ready for testing was a one hour drying cycle at 120°C to remove any residual moisture introduced during preparation. Once dry, the samples were loaded into an Instron 4484 with environmental chamber. Grips were used to hold the top and bottom of the samples at the end tabs. This approximately 3" gap length was measured for accuracy since it was used to impart constant true strain conditions in the UTM.

Stress-relaxation tests were conducted for 16 different conditions: four strain rates (0.0001 s^{-1} , 0.001 s^{-1} , 0.01 s^{-1} , and 0.05 s^{-1}) at four separate temperatures (300°C, 310°C, 320°C, and 330°C). Both the temperatures and strain rates were representative of realistic conditions imparted during the stamp forming of TuFF, hence they accurately describe elongational behavior at the ply scale. Each test was run to approximately 10% true strain, before a 30 second relaxation period commenced. During the test, a video extensometer was used to take pictures of the speckled surface during testing. Using time stamps for each frame, the images were stitched together to measure strain and strain rate ex situ. The time between frames was adjusted based on target strain rate to include between 100 and 250 images for each test.

In addition to finding the extensional viscosity of TuFF, polymer shear viscosity was also measured. Together with a constitutive model of TuFF, polymer viscosity was used to predict deformational behavior. The manufacturing of TuFF blanks used one microinch thick ULTEM

1000 PEI films, stacked in the quantities desired to reach a 57% fiber volume fraction. This same material was used in the rheological characterization of PEI.

Preparation of the PEI first consisted of stacking 40, 6" x 6" sheets together, removing any foreign materials and air bubbles between sheets. The stack was then consolidating into a 1 mm thick panel in a carver press at 20 psi and 250°C for one hour. From this panel, 25 mm disks were cut for testing in a parallel plate rheometer. Frequency oscillations ranging from 0.1 rad/s to 600 rad/s were performed at 280°C, 300°C, 330°C, and 350°C. Using time-temperature superposition (TTS) with a baseline temperature of 330°C, the shift factors were measured to produce a single curve of complex viscosity versus shear rate.

3. RESULTS

3.1 Extensional Viscosity, η_L

To analyze the extensional behavior of TuFF, longitudinal stress was calculated from the initial cross-sectional area, A_0 , the force from the load cell, and DIC strain data. Equation 3 shows this relation.

$$\sigma_L = \frac{F}{A_0}(1 + \varepsilon_L) \quad (3)$$

As mentioned previously, strain was more accurate using DIC methods as opposed to UTM data due to the reduced gauge section which overcomes the erroneous assumption of uniform strain along the length of the sample. Coupled with longitudinal strain rate data, also measured from DIC, elongational viscosity was approximated as $\eta_L \approx \frac{\sigma_L}{\dot{\varepsilon}_L}$. Figure 4 shows stress-relaxation data for the baseline test condition, $T = 330^\circ\text{C}$ and $\dot{\varepsilon}_L = 0.001 \text{ s}^{-1}$. As shown on the right in blue, stress relaxes to zero with zero strain rate, which is evidence of a viscoelastic fluid.

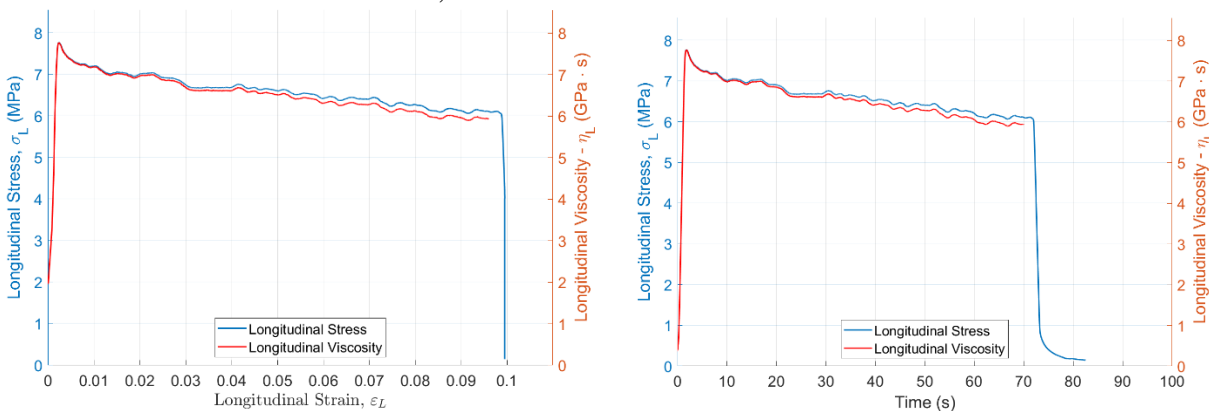


Figure 4. (Left) Stress-strain plot of a CF-PEI TuFF ply in the fiber direction at 330°C and $\dot{\varepsilon}_L = 0.001 \text{ s}^{-1}$. (Right) Stress versus time, showing stress relaxing to zero when the strain rate is zero. Red line provides the viscosity calculated using $\eta_L \approx \frac{\sigma_L}{\dot{\varepsilon}_L}$.

Figure 4 also provides the raw viscosity data for the baseline condition in red. More meaningful, however, is the viscous response to strain, strain rate, and temperature. The left graph in Figure 5 illustrates the response specifically to strain and strain rate. It is simultaneously evident that there is little strain dependence and considerable strain rate dependence. Hence, strain rate dependence is a dominant factor in determining TuFF viscosity. Nevertheless, there is still variation in viscosity based on strain, especially at higher strain rates. To normalize this variability, average viscosity

for the different strain rate conditions was calculated between 1% and 2% strain. This strain range was selected based on the relatively constant viscosity values across the range. Additionally, accurate average strain rate across the window shown in Figure 3 was calculated using DIC. Using these values, the effects of temperature were considered as shown in the right plot of Figure 5. When graphing $\log(\eta_L)$ versus $\log(\dot{\epsilon}_L)$, linear behavior was observed. The negative slope fit a power law model which was indicative of a shear thinning material.

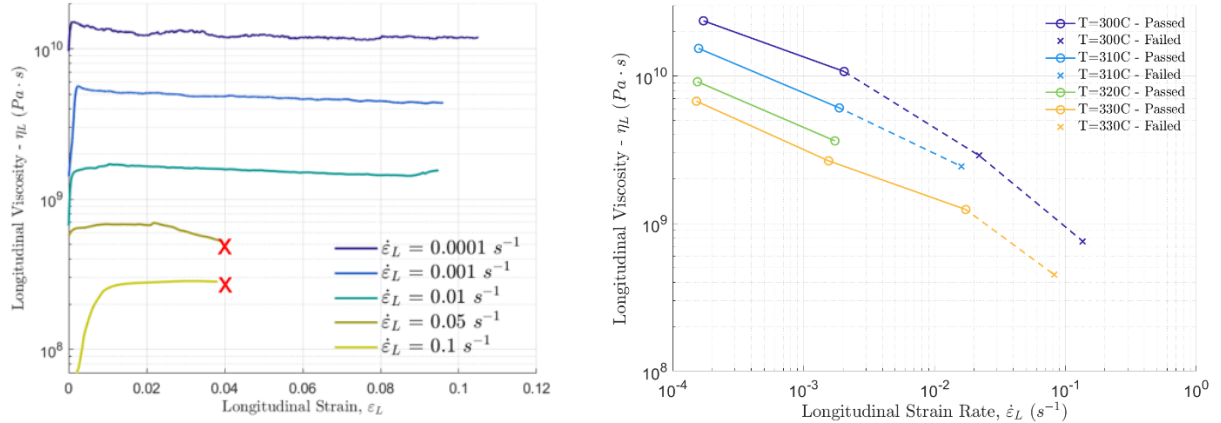


Figure 5. (Left) Fiber direction viscosity of CF-PEI TuFF at 330°C for various strain rates. Viscosity is approximately constant with strain, but changes with strain rate. (Right) Using average viscosity and strain rate values, a power law fluid behavior is observed.

To better model the strain rate and temperature dependence of TuFF, average viscosity data was fit to a plane of $1/T$ versus $\log(\eta_L)$ versus $\log(\dot{\epsilon}_L)$. This data was then mapped to the power law fluid model with an Arrhenius equation substitution as shown in Equation 4.

$$\eta_L = A e^{\frac{E}{RT}} \dot{\epsilon}_L^{n-1} \quad (4)$$

In this equation, A is the pre-exponential, E is the activation energy, R is the universal gas constant, and n is the power-law index. From this fit, the following parameters were obtained.

$$A = 0.00943 \text{ Pa} \cdot \text{s}^n \quad E = 119 \text{ kJ/mol} \quad n = 0.619$$

3.2 Polymer Viscosity, η_p

In addition to the extensional viscosity, the polymer shear viscosity was also measured at a baseline temperature of 330°C. Since PEI is an amorphous thermoplastic, a Newtonian plateau was observed at low shear rates and shear thinning behavior was witness at higher shear rates. To describe the behavior, a Carreau fluid model was used as described in Equation 5. In this model, η_∞ (viscosity when shear rate is infinity) is assumed to be zero, η_0 is the zero-shear viscosity and λ is the relaxation time.

$$\frac{\eta - \eta_\infty}{\eta_0 - \eta_\infty} = (1 + (\lambda \dot{\gamma})^2)^{\frac{n-1}{2}} \quad (5)$$

While tests were conducted at four temperatures, 330°C was used as the baseline temperature to maintain consistency with the extensional viscosity testing. After applying TTS shift factors, the 330°C curve was fit to the Carreau model to yield the following parameters.

$$\eta_0 = 2550 \text{ Pa} \cdot \text{s} \quad \lambda = 0.0675 \text{ s} \quad n = 0.533$$

3.3 Constitutive Law Modeling

Figure 6 shows the experimental data for extensional and polymer viscosity, along with the Carreau fit. From previous literature, relationships have been developed to relate polymer shear viscosity to aligned discontinuous fiber extensional viscosity under Newtonian assumptions [9]. The red line in Figure 6 is a predicted upper bound for the Newtonian plateau based on these assumptions. Although the shear thinning regime is not accurately represented through this model due to insufficient assumptions, relative viscosity magnification, η_L/η_p , is on the correct order of observed extensional viscosity data and is greater than the highest viscosity measured. Nonetheless, experimental extensional viscosity only exhibited shear thinning behavior, hence the zero-shear viscosity in TuFF is still unknown. Further testing must be conducted at lower strain rates to locate this value.

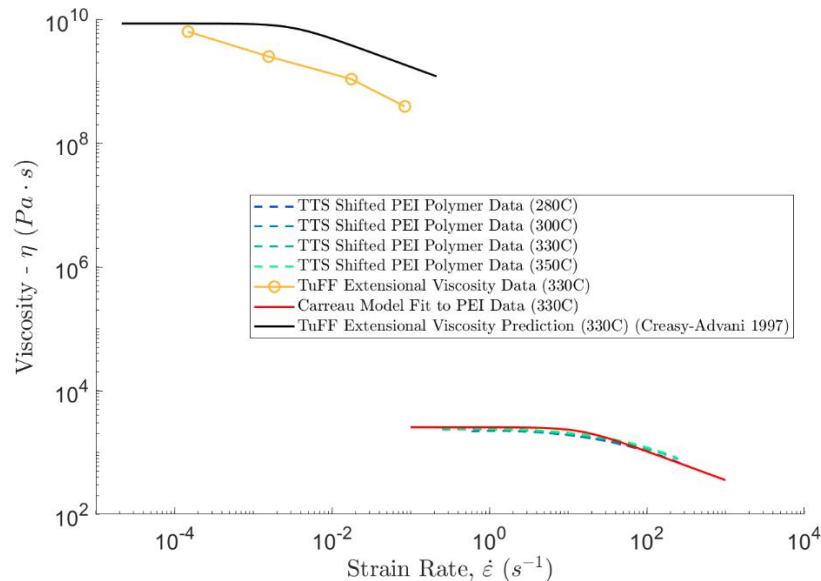


Figure 6. Polymer η_p and extensional viscosity η_L versus strain rate for a baseline temperature of 330°C. TTS shifted polymer data was used to construct the Carreau model, shown in red. The black line shows predicted TuFF viscosity under Newtonian assumptions, which sets an appropriate upper bound to the TuFF viscosity data in orange [9].

4. CONCLUSIONS

Superior strength, stiffness, and recyclability have already been shown for TuFF as compared to short and continuous fiber composites. However, this is not sufficient on its own to replace the market of continuous fiber composites. The other major factor is formability. In characterizing the material, fiber direction TuFF extensional viscosity was calculated to characterize the effects of stretch forming. Extensional viscosity was measured at temperatures and strain rates consistent with the stamp forming processes used to produce parts. Using novel DIC methods, the surface strain was measured during extension. This local precision resulted in more accurate strain and strain rate data. Rather than incorporate the entire sample, this method reduced the gauge section to a small portion within the center of the sample, which improved the accuracy of extensional viscosity data. Additionally, given the discontinuous nature of the material, DIC analysis resulted in a deeper understanding of variability in local strain data as a result of short fiber lengths.

From force and time data, stress relaxed to zero with zero strain which was indicative of a viscoelastic fluid. Considering the dominant influence of strain rate on viscosity, average values were calculated and used to characterize the material as a function of both strain rate and temperature. From this data, a power law model was applied to the TuFF data. The model was validated through rheological analysis of polymer shear viscosity. Accurately fitting this data to a Carreau fluid model, shear thinning behavior with a Newtonian plateau for the polymer was characterized. Through a micromechanical approach, TuFF viscosity was related to the polymer viscosity and using an existing model and the polymer data, predicted zero-shear viscosity aligned with the experimental TuFF data. With further microstructural analysis, a robust model can be constructed to simulate TuFF behavior during stretch forming processes.

5. REFERENCES

1. Such, M., Ward, C., & Potter, K. (2014). Aligned Discontinuous Fibre Composites: A Short History. *Journal of Multifunctional Composites*, 2(3), 155–168. <https://doi.org/10.12783/issn.2168-4286/2/3/4>
2. Yarlagadda, S., Deitzel, J., Heider, D., Tierney, J., & Gillespie, J. W. (2019). *TAILORABLE UNIVERSAL FEEDSTOCK FOR FORMING (TUFF): OVERVIEW AND PERFORMANCE*.
3. Heider, D., Tierney, J., Henchir, M. A., Gargitter, V., Yarlagadda, S., Gillespie, J. W., Sun, J., Sietins, J. M., & Knorr, D. (2019). *MICROSTRUCTURAL EVALUATION OF ALIGNED, SHORT FIBER TUFF MATERIAL*.
4. Heider, D., Tierney, J., Deitzel, J., Kubota, M., Thiravong, J., Gargitter, V., Burris, W., Morris, J., Shevchenko, N., Yarlagadda, S., & Gillespie, J. W. (2019). *CLOSED LOOP RECYCLING OF CFRP INTO HIGHLY ALIGNED HIGH PERFORMANCE SHORT FIBER COMPOSITES USING THE TUFF PROCESS*.
5. *Hexcel 8552 IM7 Unidirectional Prepreg 190 gsm & 35%RC Qualification Material Property Data Report FAA Special Project Number SP4614WI-Q Test Panel Fabrication Facility*. (2019). https://www.wichita.edu/industry_and_defense/NIAR/Documents/Qual-CAM-RP-2009-015-Rev-B-Hexcel-8552-IM7-MPDR-04.16.19.pdf
6. Revolutionizing Aircraft Materials and Processes. (2020). In *Revolutionizing Aircraft Materials and Processes*. Springer International Publishing. <https://doi.org/10.1007/978-3-030-35346-9>
7. Yarlagadda, S., Advani, S., Deitzel, J., Heider, D., Molligan, D., Roseman, D., Simacek, P., Tierney, J., & Gillespie, J. W. (2019). *FORMABILITY OF TUFF COMPOSITE BLANKS*.
8. Šimáček, P., & Advani, S. G. (2019). A micromechanics model to predict extensional viscosity of aligned long discontinuous fiber suspensions. *International Journal of Material Forming*, 12(5), 777–791. <https://doi.org/10.1007/s12289-018-1447-y>
9. Creasy, T. S., & Advani, S. G. (1997). A model long-discontinuous-fiber filled thermoplastic melt in extensional flow. *Journal of Non-Newtonian Fluid Mechanics*, 73(3), 261–278. [https://doi.org/10.1016/S0377-0257\(97\)00045-1](https://doi.org/10.1016/S0377-0257(97)00045-1)

6. ACKNOWLEDGEMENTS

This material is based upon work supported by the National Aeronautics and Space Administration under Grant and Cooperative Agreement No. 80NSSC20M0164, issued through the Aeronautics Research Mission Directorate, Transformative Aeronautics Concepts Program, University Leadership Initiative.